Photophysics and Deactivation Pathways of Thymine

Gunther Zechmann*,† and Mario Barbatti*,‡

Physical and Theoretical Chemistry Laboratory, Oxford University, South Parks Road, Oxford OX1 3QZ, U.K., and Institute for Theoretical Chemistry, University of Vienna, Währingerstraβe 17, A-1090 Vienna, Austria

Received: May 15, 2008; Revised Manuscript Received: June 20, 2008

Combined complete active space perturbation theory (CASPT2) and multireference configuration interaction calculations with single and double excitations (MR-CISD) were performed in order to explore possible deactivation pathways of thymine after photoexcitation. Equilibrium geometries are reported together with a total of eight extremes (minima or maxima) on the crossing seam (MXS), through which such radiationless transitions may occur. Furthermore, conformational analysis allows grouping these conical intersections in five distinct types. Reaction paths were calculated connecting the S_1 $^1n\pi^*$ minimum with the lowest-energy MXS of each group. Two distinct types of paths were observed, both with features that should delay the internal conversion to the ground state. This is shown to provide a possible explanation for the relatively long excited-state lifetime of thymine.

1. Introduction

A characteristic feature of the photophysics of nucleobases is their strong UV absorption due to the aromatic character and their low quantum yield of fluorescence.[1,2] This indicates the existence of ultrafast nonradiative processes which quench the fluorescence with particular efficiency.[3−9] The exceptionally short lifetimes of the UV-absorbing states of nucleobases are tentatively explained by the existence of reaction paths that connect the first singlet excited state with the singlet electronic ground state by means of conical intersections. These conical intersections form funnels, allowing ultrafast, radiationless transition to the ground state.

In experiments, remarkable success has been achieved by femtosecond laser spectroscopy investigations yielding excited-state lifetimes and short-time kinetic information,[3,9,10] but the details of the reaction mechanisms are not directly accessible by experiment. However, thorough theoretical studies are able to provide this information in the form of the analysis of energy surfaces and dynamics calculations. Considerable effort has been made by several groups in order to locate conical intersections as well as reaction paths connecting the Franck−Condon region to them for all nucleobases.[8,11−19]

Among all nucleobases (adenine, guanine, thymine, cytosine, and uracil), it is thymine that exhibits the longest excited-state lifetime, which was determined by Canuel et al.[9] and Kang et al.[3] using femtosecond resolved pump−probe ionization to be 5.2 and 6.4 ps, respectively, for 267 nm (4.64 eV) excitation energy. According to Canuel et al.,[9] this lifetime is composed of an ultrashort step (105 fs) and a longer step that accounts for 5.12 ps. The ultrashort step has been interpreted either as an indication of direct deactivation to the ground state of a fraction of the population[20] or as a $\pi\pi^*/n\pi^*$ state switch. Such dark $n\pi^*$ relay states were reported in a number of theoretical investigations in which vertical excitation energies for thymine were presented.[7,15,21−27]

In order to explain the longer step in the deactivation process, Perun et al.[15] have reported three extremes on the S_0/S_1 seam of conical intersections (MXS). All their structures support the suggestion of ring-puckered MXS. They could show by linear interpolation of internal coordinates at the CASPT2 level of theory that there exists a reaction path from the first $^1\pi\pi^*$ state to one of the MXS that exhibits only a negligibly small activation barrier, allowing for direct relaxation back to the ground state. Besides this path, Merchán et al.[14] have also explored the reaction path to the same conical intersection starting at the $^1n\pi^*$ minimum. Hudock et al.[28] could show by means of dynamics simulations that the bright S_2 state exhibits a minimum between the Franck−Condon region and the S_2/S_1 conical intersection. The relaxation of thymine into this minimum has the important effect of retarding the relaxation into the S_1 in comparison to the other nucleobases,[19] although it alone cannot possibly explain values as long as 5 ps.[9] Moreover, the relaxation into the S_2 minimum implies that the direct diabatic reaction path characterized by Merchán et al.[14] and Perun et al.[15] might not be activated and that new reaction paths taking this feature into account should be searched. As an alternative approach to explore the deactivation of thymine, several mechanisms of intersystem crossing have been carefully characterized by Serrano-Pérez et al.[18]

The current investigation shall contribute to the elucidation of photophysics by means of the quest for conical intersections and possible deactivation mechanisms. Particularly, we want to address the question of why the excited-state lifetime of thymine is comparably long.

This paper is organized as follows: After a brief technical section, which will explain the computational methods used, we will report on the stationary points found on the lowest two potential energy surfaces (PES). In section 3.2, the S_0/S_1 MXSs are discussed. Reaction paths connecting a stationary point on S_1 surface to the MXSs are presented in section 3.3 and the photodeactivation of thymine is discussed in section 3.4, followed by a concluding section of our investigations.

* Corresponding authors. E-mail addresses: gunther.zechmann@chem.ox.ac.uk, mario.barbatti@univie.ac.at.
† Oxford University.
‡ University of Vienna.

10.1021/jp804309x CCC: $40.75
Published on Web 08/15/2008

2. Computational Details

Complete active space self-consistent field (CASSCF) and multireference configuration interaction calculations with single and double excitations (MR-CISD) were carried out in order to obtain vertical excitation energies, stationary points, and MXSs. In the CASSCF calculations, state-averaging was performed with equal weights over the ground state and the lowest two excited states, one of $^1n\pi^*$ and one of $^1\pi\pi^*$ character, unless indicated otherwise. This will be denoted by SA-3. The complete active space was chosen to consist of 12 electrons in 9 orbitals [CAS(12,9), 2520 configuration state functions (CSFs)]. Active spaces comprising 6 electrons and 6 orbitals [CAS(6,6), 175 CSFs] and 14 electrons and 10 orbitals [CAS(14,10), 4950 CSFs] have also been used.

The molecular orbital (MO) expansion coefficients of the CASSCF(12,9) calculation were used for the subsequent MR-CISD calculations, in which a reference space comprising four electrons in three π and one n orbitals was chosen and will be denoted by MR-CISD(4,4). This choice can be justified by the fact that all orbitals with natural orbital occupation numbers between 0.1 and 1.9 in the CASSCF calculations were taken into the reference space. This criterion was checked for various points on the PES, including strongly distorted MXS structures. The results of this technical investigation may be found in Table S2 of the Supporting Information. The configurations of the reference wave function and all single and double excitations thereof were used for the final expansion space in terms of CSFs. The interacting space restriction suggested by Bunge[29] was imposed on all MRCI calculations. In all post-MCSCF calculations, the 1s core orbitals of the nine heavy atoms were kept frozen. As the MRCI method is not inherently size-extensive, corrections to the CI energies were taken into account by the correction suggested by Pople et al.[30] and will be denoted by $+Q$.

Linear interpolation of internal coordinates[31] (LIIC) was used to calculate reaction paths between the minimum in the S_1 state and the MXSs optimized at the MR-CISD level. Single point calculations were performed at the complete active space second-order perturbation theory level using 14 electrons, 10 orbitals, and 5 states in the state averaging procedure [CASPT2/CASSCF(14,10)] using the 6−31G* basis set. No level shift was necessary. An IPEA shift of 0.25 was included.[32]

For the equilibrium ground-state geometry, benchmark calculations were performed with the equation of motion coupled cluster method including single and double excitations (EOM-CCSD).[33] This was done for the excitation energies and oscillator strengths, for which the possibility to yield highly accurate results for electronic transitions dominated by single excitations was shown by Stanton and Bartlett.[33]

In the present work, we mainly use two basis sets. The 6−31G* Pople-type basis[34] has generally been accepted as a good compromise between accuracy and computational costs in a large number of applications. Due to the relatively large size of the molecule, the high computational demand of the MR-CISD method and the aim of dynamics calculations in future investigations, however, we have also used the rather modest 3−21G basis set.[35] This was done after careful comparison and validation of geometries and excitation energies with different methods and we will present comparative results about the validity of this ansatz in section 3 of this work, which includes benchmark data up to the polarized triple-ζ quality 6−311G** basis set.[36]

For the purpose of systematic classification of the conical intersections, we have adopted the Cremer-Pople approach (CP),[37,38] which is designed to give a mathematically well defined description of the shape of a puckered ring. In this approach, the internal coordinates of an N-membered ring are projected onto a subspace of N-3 coordinates (or parameters). Each point in this subspace corresponds to a different conformation. The conformation can be further classified in terms of the six canonical puckered rings, namely, chair (C), boat (B), envelope (E), screw-boat (S), half-chair (H), and twist-boat (T) as proposed by Boeyens[39] based on the polar set of CP parameters Q, θ, ϕ.[37]

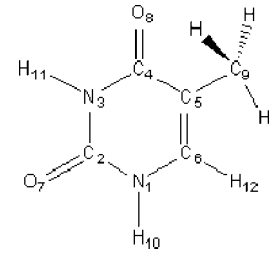

Figure 1. Structure and labeling of thymine.

Geometry optimizations performed at the MRCI and CASSCF levels used the analytical gradients described in refs 40−42. Analytical nonadiabatic coupling vectors[43,44] were computed as implemented in the COLUMBUS program[45−47] for the calculation of extremes on the crossing seam.

For the EOM-CCSD calculations, the ACES II program was used.[48] All CASSCF and MR-CISD calculations were performed with the COLUMBUS program with AO integrals and AO gradient integrals taken from the DALTON program.[49] The MP2/SV(P) and DFT/TZ calculations were carried out with the TURBOMOLE program package,[50,51] while the CASPT2 calculations were performed with the Molcas 6.4 package.[52]The CP parameters were obtained with the PLATON program.[53]

3. Results and Discussion

All geometries reported in this section were optimized without symmetry restrictions at CASSCF(6,6) level with the 6−31G* and the 3−21G basis sets and at the MR-CISD(4,4)/SA-3-CAS(12,9) level with the 3−21G basis set. The corresponding Cartesian coordinates may be found in the Supporting Information. The labeling and default conformation of the atoms in thymine, which will be used throughout this work, are defined as presented in Figure 1.

3.1. Stationary Points of the S_0 and S_1 States. The starting geometry for the ground state was chosen such that two of the hydrogen atoms in the methyl group point toward the neighboring oxygen atom. Although a local minimum with the opposite conformation exists, the current choice has proven to be slightly lower in energy by 0.07 eV based on MP2/SV(P) and by 0.04 eV based on DFT(B3LYP)/TZ calculations. The resulting minimum structure is practically of C_s symmetry.

EOM-CCSD results at the ground-state equilibrium geometry are presented in Table 1, where excitation energies and oscillator strengths are shown up to the S_4 state with the 6−311G**, 6−31G*, and 3−21G basis sets. Augmentation of the basis set to triple-ζ quality and inclusion of polarization functions on hydrogen atoms did not show any influence larger than 0.07 eV at an average for the four lowest excited states as compared to the 6−31G* calculations. This modest basis set dependence of excitation energies (and oscillator strengths) is in agreement with previous observations.[33]

Along with the EOM-CCSD excitation energies, corresponding CASPT2 and experimental results[54] are shown. Excitation

TABLE 1: Vertical Excitation Energies and Oscillator Strengths Obtained with the EOM-CCSD and the CASPT2 Methods up to the S_4 State[a]

		EOM/6−311G** [b]		EOM/6−31G* [c]		EOM/3−21G [d]		CASPT2/6−31G* [e]		exp.[f]
state	character	ΔE (eV)	ΔE (eV)	osc. str.	osc. str.	ΔE (eV)	osc. str.	ΔE (eV)	osc. str.	ΔE (eV)
S_1	$^1n\pi^*$	5.25	5.29	9.01×10^{-5}	5.77×10^{-5}	5.24	4.49×10^{-4}	5.11 (4.90)	5.00×10^{-3}	
S_2	$^1\pi\pi^*$	5.69	5.80	1.69×10^{-1}	1.72×10^{-1}	6.03	1.72×10^{-1}	5.38 (4.97)	1.95×10^{-1}	4.95 ± 0.08
S_3	$^1n\pi^*$	6.70	6.73	1.34×10^{-5}	1.05×10^{-5}	6.71	2.19×10^{-5}	6.57 (6.17)	0.00	
S_4	$^1\pi\pi^*$	6.94	7.04	4.74×10^{-2}	4.54×10^{-2}	7.08	6.33×10^{-2}	6.60 (6.34)	1.27×10^{-1}	6.2 ± 0.08

[a] CASPT2 values with IPEA = 0 are given in parentheses. [b] EOM - EOM-CCSD; E_0(EOM-CCSD/6−311G**) = −453.063673 au. [c] EOM - EOM-CCSD; E_0(EOM-CCSD/6−31G*) = −452.826817 au. [d] EOM - EOM-CCSD; E_0(EOM-CCSD/3−21G) = −449.902341 au. [e] E_0(CASPT2/CASSCF(14,10)/6−31G*) = −452.798940 au (−452.802490 au). [f] Electron energy loss spectroscopy, gas phase, ref 54.

TABLE 2: Transition Energies of Stationary Points and MXSs Calculated at the CASPT2, MR-CISD, and MR-CISD+Q (in parenthesis) Levels Relative to the Ground State Minimum[a]

		ΔE (eV)	
geometry	state/character	MR-CISD(+Q)	CASPT2
S_0 Min.	S_0 $^1\pi^2$	0.00 (0.00)[b]	0.00[c]
S_0 Min.	S_1 $^1n\pi^*$	5.26 (5.07)	5.11
S_0 Min.	S_2 $^1\pi\pi^*$	6.94 (6.08)	5.38
S_1 Min.	S_0 $^1\pi^2$	1.65 (1.22)	1.48
S_1 Min.	S_1 $^1n\pi^*$	4.01 (4.28)	4.60
S_1 Min.	S_2 $^1\pi\pi^*$	7.06 (5.64)	5.37
	Type I		
MXS1 (E_5)	$^1\pi^2/^1\pi\pi^*$	4.80 (4.49/4.68)[d]	4.51/4.66[d]
	Type II		
MXS2 (^6E)	$^1\pi^2/^1\pi\pi^*$	5.41 (5.01/5.30)	4.91/5.16
MXS5 ($\sim^6E$)	$^1\pi^2/^1\pi\pi^*$	6.08 (5.11/6.19)	5.10/6.35
MXS7 ($\sim^6S_1$)	$^1\pi^2/^1\pi\pi^*$	6.85 (6.28/6.30)	6.20/6.38
	Type III		
MXS3 ($B_{4,1}$)	$^1\pi^2/^1n\pi^*$	4.80 (3.93/4.49)	4.93/5.32
	Type IV		
MXS4 ($^{6,3}B$)	$^1\pi^2/^1n\pi^*$	4.92 (4.45/5.11)	5.78/6.03
MXS8 ($B_{6,3}$)	$^1(\pi^2+\pi\pi^*)/^1n\pi^*$	5.61 (5.38/5.41)	5.54/5.74
	Type V		
MXS6 ($^3T_1$)	$^1\pi^2/^1\pi\pi^*$	6.08 (5.65/6.12)	5.65/6.12

[a] The MXSs have been collected in groups according to the criteria discussed in the text. The notation for the puckered conformations are E, envelope; S, screw-boat; B, boat; T, twist-boat. [b] E_0(MR-CISD-(4,4)/SA-3-CAS(12,9)/3−21G) = −449.7180357 au (+Q = −449.904773 au). [c] E_0(CASPT2/CASSCF(14,10)/6−31G*) = −452.798940 au. [d] S_0/S_1 energies. The energy split occurs because the methods used for energy calculation and MXS optimization differ.

energies at the MRCI (+Q) level are given in Table 2. A longer compilation of previous theoretical results for vertical excitation energies is given in Table S1 of the Supporting Information. As can be seen, the state ordering is consistently reproduced for all methods that we have used and the excitation energies are in good agreement, even though the CASPT2 results are slightly lower by about 0.2 eV as compared to our largest EOM-CCSD calculation. This is a general tendency in the comparison between these two methods discussed in detail in ref 55. Although somewhat lower than the EOM-CCSD results, the CASPT2 excitation energies are a few tenths of an eV higher than previous CASPT2 results.[15,18,21] The reason for that is due to the usage of the IPEA shift[32] mentioned in the Computational Details section. If the conventional noncorrected perturbative Hamiltonian is used (Table 1, in parentheses), our results are in good agreement with the previous CASPT2 energies.[15,18,21] As usual,[56] the $^1\pi\pi^*$ energy at the MRCI level is too high and much larger CI expansions would be necessary to correct it.

For the first excited $^1n\pi^*$ S_1 minimum, even though it was optimized in C_1 symmetry, we also obtain a planar structure

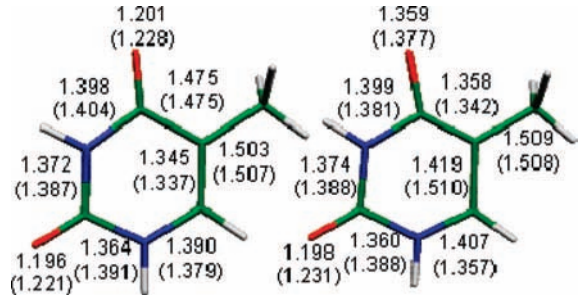

Figure 2. CASSCF(6,6)/6−31G* (MR-CISD(4,4)/CASSCF(12,9)/3−21G) optimized structures of the S_0 equilibrium ground state (left) and the S_1 $^1n\pi^*$ minimum (right). Distances between heavy atoms are in given Ångströms.

(see Figure 2) with geometric parameters similar to the minimum reported in ref 15. As we can see from the bond lengths in Figure 2, the $n\pi^*$ excitation is localized primarily around the C_5-C_6 and C_4-O_8 bonds, which are stretched and bent away from the methyl tetrahedron, whereas the C_2-O_7 bond remains unaffected. Energies for the S_1 minimum geometry at the CASPT2 and MRCI levels are given in Table 2, from which one can observe the strong relaxation of the $^1n\pi^*$ state in comparison to its energy at the ground-state equilibrium geometry.

3.2. Conical Intersections. In order to find the extremes on the seam of conical intersections, we have generated several starting geometries according to the procedure suggested in ref 57. This results in puckered structures, which have frequently been observed to lead to MXS.[8,11,12,57−59] In a first step, we have optimized these initial geometries with the CASSCF method. In these calculations, state averaging was performed over the two intersecting states. Overall, we obtained eight MXS geometries with both basis sets (6−31G* and 3−21G), which are shown in Figure S1 of the Supporting Information. Six of these conical intersections have not been previously described.

In the next step, we used these structures for optimizations at the aforementioned MR-CISD level. This yielded a total of eight MR-CISD structures of conical intersections, which are illustrated in Figure 3. One can see that the conformational deviations caused by the different basis sets (Figure S1 of the Supporting Information) are of same order as the changes resulting from the improved description of static and dynamical correlations (Figure 3 and Figure S1). In both cases, the standard deviation of the bond distance changes is about 0.02 Å.

The MXS 1 is similar to the optimized CI_1 and the $(gs/\pi\pi^*)_{CI}$ intersections reported, respectively, by Perun et al.[15] and Merchán et al.[14] Its conformation, as revealed by the Cremer-Pople parameters (see Table 3 and Table S3 in the Supporting Information), is an envelope puckered at C_5 atom (E_5). Two other MXSs (numbers 2 and 7 in Figure 3) show puckering of the C_6 carbon as the main structural feature, corresponding to envelope ^6E and screw-boat $^6S_1$ conformations, respectively. In

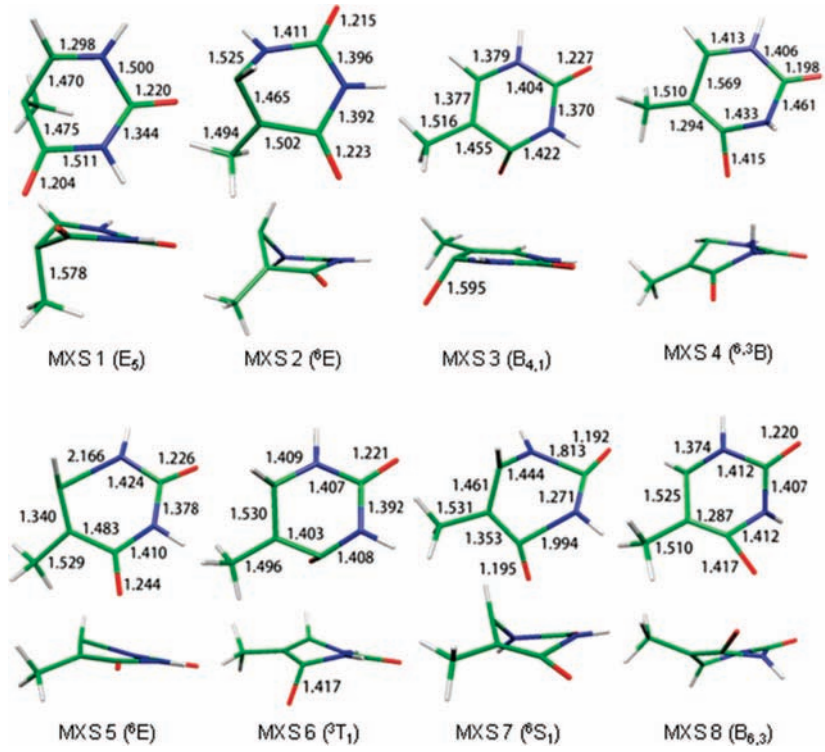

Figure 3. MR-CISD(4,4)/SA-3-CAS(12,9)/3−21G optimized structures of the eight MXS. Distances between heavy atoms are given in angström. Structures and distances optimized at CASSCF(6,6) with 6−31G* and 3−21G basis sets are given in Figure S1 of the Supporting Information.

TABLE 3: Cremer-Pople Parameters and Conformations for the MXSs at the MRCI Level[a]

geometry	Q (Å)	θ (°)	φ (°)	conformation
Type I				
MXS1	0.474	113.8	59.6	E_5
CI_1 [b]	0.387	110.9	88.8	$^6S_5$
CI_3 [b]	0.661	119.4	70.6	E_5
$(gs/\pi\pi^*)_{CI}$ [c]	0.456	107.3	81.3	$^6S_5$
Type II				
MXS2	0.761	115.6	116.9	^6E
MXS5	D	–	–	$\sim {}^6E$
MXS7	D	–	–	$\sim {}^6S_1$
Type III				
MXS3	0.100	79.4	179.6	$B_{4,1}$
Type IV				
MXS4	0.520	84.6	120.2	$^{6,3}B$
MXS8	0.371	87.3	289.9	$B_{6,3}$
Type V				
MXS6	0.451	90.1	139.9	$^3T_1$
CI_2[b]	0.608	99.5	138.3	$^3T_1$

[a] D - dissociated structure. [b] MXS structures of ref 15. [c] MXS structure of ref 14.

the MXS 7, substantial elongation up to ~2 Å of the N_1-C_2 and N_3-C_4 bonds should be pointed out. This remarkable characteristic also occurs in the N_1-C_6 bond of MXS 5, but with only slight puckering contributions around the C_6 atom. Conical intersections with similar CN bond elongation have also been reported for adenine and pyrrole.[60,61] In MXS 3, the ring is kept almost planar while the O_4 atom is strongly displaced out of the ring plane. Such a conical intersection has also been described in cytosine[8] and pyridone[62] and it has a close analogue in formamide.[63]

MXSs 4 and 6 are conformational neighbors showing the boat $^{6,3}B$ and the twisted-boat $^3T_1$ conformations, respectively. We can observe similar bond elongation of the CO-bond for both structures, and the main difference appears in the C_5O_8 bond, which is strongly pyramidalized in MXS 6 but not in MXS 4. In these two cases, substantial ring deformation is necessary to reach an intersection. The last structure shown in Figure 3 (MXS 8) shows a boat $B_{3,6}$ conformation and is similar to MXS 4. The difference between them is mainly in the degree of puckering, which is larger in MXS 4 (see puckering amplitude Q in Table 3). Other differences are in the positions of the H_{11} and H_{12} hydrogen atoms, which are in *cis* position in MXS 4 and in *trans* position in MXS 8. The CI_3 conical intersection reported in ref 15 is not among the eight conical intersection presented in this work. It corresponds to an envelope E_5 conformation, similar to MXS 1, but with a different position of the methyl group, which explain its high energy.

Energies at the CASPT2 and MRCI levels and state characters of the MXSs are given in Table 2. The energy split between S_0 and S_1 states at CASPT2 and MRCI+Q is, as usual, caused by the difference between the method used for MXS optimization and that used for single point calculation. Naturally, at MRCI level the S_0 and S_1 energies are the same. Although the energetic order of the MXSs is not exactly the same depending on the method, the results show that among the MXS structures it is the envelope conformation puckered around the C_5-atom (E_5) that lies lowest in energy and is therefore most favorable from a thermodynamic point of view. This is in agreement with recent findings of Merchán et al.[14] and Perun et al.,[15] but applies in a slightly more general context, since the number of MXS structures investigated in the present work is larger. The C_6-envelope puckered MXS2 (^6E), the oxygen out-of-plane MXS3 ($B_{4,1}$), and the boat MXS4 ($^{6,3}B$) also appear at low energies. The inclusion of Pople corrections to the MRCI energies even makes the ^6E MXS the lowest-energy structure. The energies of the $^1n\pi^*/^1\pi^2$ MXSs at CASPT2 level should be overestimated in comparison to the energies of the $^1\pi\pi^*/^1\pi^2$ MXSs due to the uphill and downhill shapes of the $^1n\pi^*$ and $^1\pi\pi^*$ surfaces,

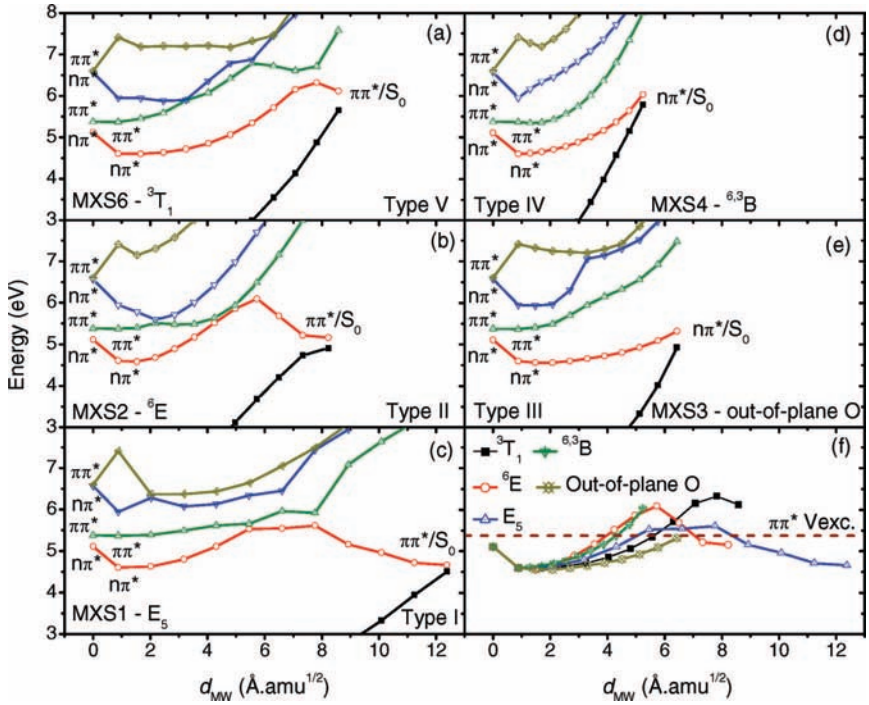

Figure 4. (a−e) LIIC paths connecting the minimum in the S_1 state (0.88 Å.amu$^{1/2}$) to the MXSs obtained at the CASPT2/CASSCF(14,10)/6−31G* level of theory. The paths are given as a function of the mass-weighted distance d_{MW} between each point and the minimum in the ground state. The first point (0.00 Å.amu$^{1/2}$) corresponds to the S_0 equilibrium geometry. (f) S_1-state curves for all paths together.

respectively, close to the intersections (see section 3.3). The remaining MXSs occur at somewhat higher energies and may play important roles when excitations to higher electronic states are considered.

Since the crossing seam of thymine presents a complex structure involving several different local minima, it is useful to group these MXSs into five types (see Table 2 and Table 3) based on the analysis of their geometries and state character. In the first type (type I), the conical intersections are puckered at the C_5 atom, which pushes the methyl group out of the ring plane. Conical intersections identified as CI_1 and CI_3 in ref 15 belong to this type and the main difference between them is the degree of puckering, which is larger in CI_3. The conical intersection $(gs/\pi\pi^*)_{CI}$ reported in ref 14 also belongs to this type. In type II, the conical intersections show puckering at the C_6 atom. Two of the MXSs included in this type show dissociative behavior of the N−C bonds. Type III features conical intersections with planar and semiplanar rings and strongly out-of-plane oxygen atom, while type IV includes MXSs puckered at N_3 and C_6 with boat conformation. Finally, type V is composed of MXSs puckered at the N_1 and N_3 atoms. The conical intersection identified as CI_2 in ref 15 belongs to this type.

The $^1\pi-3s(\sigma^*)/S_0$ conical intersections, which usually appear along the NH-stretching paths,[64−66] have not been investigated in this work because for thymine the vertical excitation into the $^1\pi-3s(\sigma^*)$ state is more than 0.5 eV higher than the excitation into the lowest $^1\pi\pi^*$ state.[27] This means that the activation of the NH-stretching paths should take place at higher excitation energies than those of the low-energy tail of the absorption band that have been experimentally employed[3,9] and that we are currently discussing.

3.3. Deactivation Pathways. Although the investigation of excitation energies can shed valuable light on the accessibility of points on a PES, the information we derive about the pathways that the molecule describes on its way is more than limited. Once the molecule has been pumped to one of the first bright electronically excited states, it will look for ways to move to points on the PES that are lower in energy than the Franck−Condon (FC) region.

As we have discussed in the Introduction, Hudock et al.[16] showed that thymine relaxes into the S_2 minimum and remains there for a relatively long time before decay to the S_1 state occurs. In this aspect, it differs from other aromatic heterocycles, which quickly relax to S_1 within 100 fs.[19,62,67] The equilibration in S_2 makes it reasonable to suppose that thymine reaches the S_2/S_1 crossing statistically without any bias toward some specific reaction coordinate. Therefore, from this crossing it should relax into the S_1 minimum rather than diabatically follow to the S_0/S_1 crossing discussed in refs 14 and 15. The latter effect has been observed in adenine, which quickly moves through the excited sates without either equilibrating in any excited state or changing the diabatic character until finding the S_1/S_0 crossing.[19,20]

In order to come to a more complete description of the deactivation pathways after thymine finally moves to the S_1 state, we have recorded reaction paths from the S_1 minimum to the lowest-energy MXS of each type by linear interpolation of internal coordinates. It should be stressed that such reaction paths are not minimum-energy paths and that energy barriers might be deceptive under this aspect, but we can at least gain helpful qualitative information about possible deactivation mechanisms. The reaction paths calculated at the CASPT2/CASSCF(14,10)/6−31G* level are shown in Figure 4a−e, whereas in Figure 4f, the potential energy curves of the S_1 state have been collected for all deactivation pathways. Although in these graphs the FC region (0.00 Å.amu$^{1/2}$) is connected to the S_1 $^1n\pi^*$ minimum (0.88 Å.amu$^{1/2}$), we should note that, as discussed above, thymine should not directly move between them, but equilibrate in the minimum of S_2 state (not shown) before.

The character of the S_1 and S_0 states for MXSs of types I, II, and V is $^1\pi\pi^*/^1\pi^2$. In all these cases, the S_1 state shows a barrier

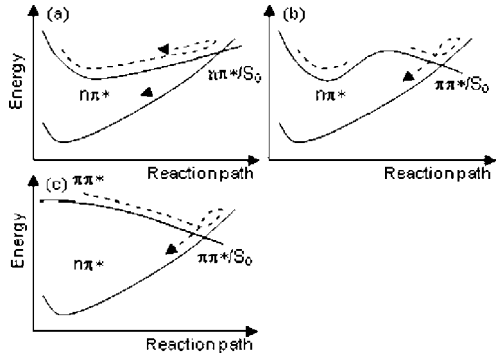

Figure 5. Schematic view of the deactivation paths in thymine along the S_1 state. In both cases, the excited-state lifetime should be elongated either because of (a) the uphill shape of the S_1 surface or (b) the barrier. The direct diabatic path (c), although available, should not be activated.

induced by the $^1n\pi^*/^1\pi\pi^*$ state crossing followed by a descent path toward the conical intersection. For MXSs of types III and IV, the S_1 and S_0 states have $^1n\pi^*/^1\pi^2$ character and the conical intersection is reached by an ascending pathway without intermediary barriers.

Due to the out-of-plane dislocation of the methyl group, the type I (E_5) conical intersections requires the largest distortions from the Franck−Condon (FC) region. It is also the lowest-energy MXS. The smallest distortions are required by type IV ($^{6,3}B$) conical intersections. Its energy is probably overestimated at CASPT2 level (see section 3.2) and it should be accessible after the excitation into the first $^1\pi\pi^*$ state. All other MXSs show similar mass-weighted distances to the FC region. The energies of the out-of-plane O (type III) and ^6E (type II) MXSs are below the vertical excitation and that of the $^3T_1$ (type V) MXS is above.

3.4. Mechanisms for Photodeactivation in Thymine. The analysis of the deactivation paths suggests the following scenario for the photodynamics of thymine. After relaxing into the S_1 state minimum, conical intersections with $^1n\pi^*/^1\pi^2$ character can be reached. Nevertheless, as schematically illustrated in Figure 5a, the ascending shape of the S_1 surface is not favorable for the nonadiabatic decay, because even if the molecule reaches the neighborhood of this intersection seam, it can quickly move to other regions of the configurational space before deactivating. For this reason, these conical intersections should be inefficient for the internal conversion. This effect has been previously observed in the dynamics of pyridone,[62] which despite the availability of $^1n\pi^*/^1\pi^2$ conical intersections turns out to be a fluorescent species.

On the other hand, in order to reach the $^1\pi\pi^*/^1\pi^2$ region of crossing seam from the S_1 minimum, a barrier caused by an avoided crossing between the $^1n\pi^*$ and $^1\pi\pi^*$ energy surfaces needs to be overcome (Figure 5b). After the barrier, however, the favorable descending shape of the $^1\pi\pi^*$ surface should keep thymine trapped in that region and the conical intersection can be found. This trapping effect, first identified in the dynamics of substituted ethylenes,[68,69] has been recently observed in dynamics simulations for adenine, which decays through paths showing similar downhill features.[19]

Were it not for the relaxation into the S_2 minimum discussed in ref 16, thymine could follow the available $^1\pi\pi^*$ diabatic path[14,15] (Figure 5c) like adenine does.[19] If this were the case, thymine would show a similarly short lifetime.

Both the uphill shape of the $^1n\pi^*$ paths and the barriers along the $^1\pi\pi^*$ paths push the excited-state lifetime of thymine to longer values than observed for the other nucleobases,[9] but still render the occurrence of internal conversion possible, which makes it a nonfluorescent species.

Note in particular that the $^1\pi\pi^*/^1\pi^2$ conical intersections in thymine request the out-of-plane displacement of the methyl group attached to C_5 (see MXS 1 and 2 in Figure 3). In uracil and also in cytosine, the same ring site is saturated by a single hydrogen atom instead. This difference seems to be enough to make the barrier on the S_1 surface quite a bit higher in thymine than in uracil and cytosine.[14] This should be the main reason for longer lifetime of thymine in comparison to the other two nucleobases.

4. Conclusions

Ab initio investigations were performed in order to elucidate processes leading to radiationless deactivation of thymine after photoexcitation. EOM-CCSD, MR-CISD, and CASPT2 methods have been employed.

The ground-state geometry and the first excited-state structure were optimized at the CASSCF and MR-CISD levels. Both minima are planar, but in the excited state the carbonyl oxygen is bent away from its neighboring the methyl group. In addition, a total of eight extremes on the crossing seam were found, from which six have not been previously reported and four are low-energy intersections that can be reached after excitation into the lowest $^1\pi\pi^*$ state. These conical intersections show different kinds of ring puckered conformations, bond elongations, and out-of-plane distortions of the carbonyl oxygen and of the methyl group. On the basis of conformational analysis, all these conical intersections have been grouped into five distinct types.

Reaction paths leading from the S_1 $^1n\pi^*$ minimum to the lowest-energy MXS of each group were obtained by linear interpolation of internal coordinates. They show that there exist two kinds of reaction deactivation paths, those involving $^1n\pi^*/S_0$ crossings and those involving $^1\pi\pi^*/S_0$ crossings. In the first case (Figure 5a), the S_1 surface in the neighborhood of the conical intersection shows an uphill shape, which implies that when thymine moves along this kind of path, it can approach the intersection and move away from it before having enough time to decay. In the second case, involving paths to $^1\pi\pi^*/S_0$ crossing (Figure 5b), due to the relaxation into the S_1 $^1n\pi^*$ minimum, thymine must overcome high energy barriers before finding the downhill section of the potential energy surface. Together, these features of the reaction paths explain why thymine has a lifetime that is much longer than the lifetime of the other nucleobases.

Acknowledgment. This work was supported by the Austrian Science Fund within the framework of the Special Research Program F16 (Advanced Light Sources) and Project P18411−N19. We are grateful for technical support and computer time at the Linux PC cluster Schrödinger III of the computer center of the University of Vienna.

Supporting Information Available: Occupation numbers of the natural orbitals, Cremer-Pople parameters and conformations for the MXSs, vertical energy excitations, MXS structures, Cartesian coordinates of stationary points and MXSs. This material is available free of charge via the Internet at http://pubs.acs.org.

References and Notes

(1) Duggan, D. E.; Bowman, R. L.; Brodie, B. B.; Udenfriend, S. *Arch. Biochem. Biophys.* **1957**, *68*, 1.

(2) Longworth, J. W.; Rahn, R. O.; Shulman, R. G. *J. Chem. Phys.* **1966**, *45*, 2930.
(3) Kang, H.; Lee, K. T.; Jung, B.; Ko, Y. J.; Kim, S. K. *J. Am. Chem. Soc.* **2002**, *124*, 12958.
(4) Kang, H.; Jung, B.; Kim, S. K. *J. Chem. Phys.* **2003**, *118*, 6717.
(5) He, Y.; Wu, C.; Kong, W. *J. Phys. Chem. A* **2004**, *108*, 943.
(6) Ullrich, S.; Schultz, T.; Zgierski, M. Z.; Stolow, A. *J. Am. Chem. Soc.* **2004**, *126*, 2262.
(7) Crespo-Hernández, C. E.; Cohen, B.; Hare, P. M.; Kohler, B. *Chem. Rev.* **2004**, *104*, 1977.
(8) Blancafort, L.; Cohen, B.; Hare, P. M.; Kohler, B.; Robb, M. A. *J. Phys. Chem. A* **2005**, *109*, 4431.
(9) Canuel, C.; Mons, M.; Piuzzi, F.; Tardivel, B.; Dimicoli, I.; Elhanine, M. *J. Chem. Phys.* **2005**, *122*, 074316.
(10) Satzger, H; Townsend, D; Zgierski, M. Z; Patchkovskii, S; Ullrich, S; Stolow, A *Proc. Natl. Acad. Sci. U.S.A.* **2006**, *103*, 10196.
(11) Matsika, S. *J. Phys. Chem. A* **2004**, *108*, 7584.
(12) Marian, C. M. *J. Chem. Phys.* **2005**, *122*, 104314.
(13) Zgierski, M. Z.; Patchkovskii, S.; Fujiwara, T.; Lim, E. C. *J. Phys. Chem. A* **2005**, *109*, 9384.
(14) Merchán, M.; Gonzalez-Luque, R.; Climent, T.; Serrano-Andrés, L.; Rodriuguez, E.; Reguero, M.; Pelaez, D. *J. Phys. Chem. B* **2006**, *110*, 26471.
(15) Perun, S.; Sobolewski, A. L.; Domcke, W. *J. Phys. Chem. A* **2006**, *110*, 13238.
(16) Hudock, H. R.; Levine, B. G.; Thompson, A. L.; Satzger, H.; Townsend, D.; Gador, N.; Ullrich, S.; Stolow, A.; Martinez, T. J. *J. Phys. Chem. A* **2007**, *111*, 8500.
(17) Marian, C. M. *J. Phys. Chem. A* **2007**, *111*, 1545.
(18) Serrano-Pérez, J. J.; Gonzalez-Luque, R.; Merchán, M.; Serrano-Andrés, L. *J. Phys. Chem. B* **2007**, *111*, 11880.
(19) Barbatti, M.; Lischka, H. *J. Am. Chem. Soc.* **2008**, *130*, 6831.
(20) Serrano-Andrés, L; Merchán, M.; Borin, A. C *Proc. Natl. Acad. Sci. U.S.A.* **2006**, *103*, 8691.
(21) Lorentzon, J.; Fulscher, M. P.; Roos, B. O. *J. Am. Chem. Soc.* **1995**, *117*, 9265.
(22) Broo, A.; Holmen, A. *J. Phys. Chem. A* **1997**, *101*, 3589.
(23) Shukla, M. K.; Leszczynski, J. *J. Comput. Chem.* **2004**, *25*, 768.
(24) Wesolowski, T. A. *J. Am. Chem. Soc.* **2004**, *126*, 11444.
(25) Tsolakidis, A.; Kaxiras, E. *J. Phys. Chem. A* **2005**, *109*, 2373.
(26) Gustavsson, T.; Banyasz, A.; Lazzarotto, E.; Markovitsi, D.; Scalmani, G.; Frisch, M. J.; Barone, V.; Improta, R. *J. Am. Chem. Soc.* **2006**, *128*, 607.
(27) Fleig, T.; Knecht, S.; Hättig, C. *J. Phys. Chem. A* **2007**, *111*, 5482.
(28) Hudock, H. R.; Levine, B. G.; Thompson, A. L.; Satzger, H.; Townsend, D.; Gador, N.; Ullrich, S.; Stolow, A.; Martinez, T. J. *J. Phys. Chem. A* **2007**, *111*, 8500.
(29) Bunge, A. *J. Chem. Phys.* **1970**, *53*, 20.
(30) Pople, J. A.; Seeger, R.; Krishnan, R *Int. J. Quantum Chem.* **1977**, *11*, 149.
(31) Fogarasi, G.; Zhou, X. F.; Taylor, P. W.; Pulay, P. *J. Am. Chem. Soc.* **1992**, *114*, 8191.
(32) Ghigo, G.; Roos, B. O.; Malmqvist, P.-A. *Chem. Phys. Lett.* **2004**, *396*, 142.
(33) Stanton, J. F.; Bartlett, R. J. *J. Chem. Phys.* **1993**, *98*, 7029.
(34) Hehre, W. J; Ditchfie, R; Pople, J. A *J. Chem. Phys.* **1972**, *56*, 2257.
(35) Binkley, J. S.; Pople, J. A.; Hehre, W. J. *J. Am. Chem. Soc.* **1980**, *102*, 939.
(36) Krishnan, R.; Binkley, J. S.; Seeger, R.; Pople, J. A. *J. Chem. Phys.* **1980**, *72*, 650.
(37) Cremer, D.; Pople, J. A. *J. Am. Chem. Soc.* **1975**, *97*, 1354.
(38) Cremer, D. *Acta Crystallogr., Sect. B: Struct. Sci.* **1984**, *40*, 498.
(39) Boeyens, J. C. A. *J. Chem. Crystallogr.* **1978**, *8*, 317.
(40) Shepard, R. The Analytic Gradient Method for Configuration Interaction Wave Functions. In *Modern Electronic Structure Theory*; Yarkony, D. R., Ed.; World Scientific: Singapore, 1995; Vol. 1, p 345.
(41) Shepard, R.; Lischka, H.; Szalay, P. G.; Kovar, T.; Ernzerhof, M. *J. Chem. Phys.* **1992**, *96*, 2085.
(42) Lischka, H.; Dallos, M.; Shepard, R. *Mol. Phys.* **2002**, *100*, 1647.
(43) Lischka, H.; Dallos, M.; Szalay, P. G.; Yarkony, D. R.; Shepard, R. *J. Chem. Phys.* **2004**, *120*, 7322.
(44) Dallos, M.; Lischka, H.; Shepard, R.; Yarkony, D. R.; Szalay, P. G. *J. Chem. Phys.* **2004**, *120*, 7330.
(45) Lischka, H.; Shepard, R.; Brown, F. B.; Shavitt, I *Int. J. Quantum Chem.* **1981**, *15*, 91.
(46) Lischka, H.; Shepard, R.; Pitzer, R. M.; Shavitt, I.; Dallos, M.; Müller, T.; Szalay, P. G.; Seth, M.; Kedziora, G. S.; Yabushita, S.; Zhang, Z. Y. *PhysChemChemPhys* **2001**, *3*, 664.
(47) Lischka, H.; Shepard, R.; Shavitt, I.; Pitzer, R. M.; Dallos, M.; Müller, T.; Szalay, P. G.; Brown, F. B.; Ahlrichs, R.; Boehm, H. J.; Chang, A.; Comeau, D. C.; Gdanitz, R.; Dachsel, H.; Ehrhardt, C.; Ernzerhof, M.; Höchtl, P.; Irle, S.; Kedziora, G.; Kovar, T.; Parasuk, V.; Pepper, M. J. M.; Scharf, P.; Schiffer, H.; Schindler, M.; Schüler, M.; Seth, M.; Stahlberg, E. A.; Zhao, J.-G.; Yabushita, S.; Zhang, Z.; Barbatti, M.; Matsika, S.; Schuurmann, M.; Yarkony, D. R.; Brozell, S. R.; Beck, E. V.; Blaudeau, J.-P. *COLUMBUS, an ab initio electronic structure program*, release 5.9.1; 2006; www.univie.ac.at/columbus.
(48) Stanton, J. F.; Gauss, J.; Watts, J. D.; Lauderdale, W. J.; Bartlett, R. J *Int. J. Quantum Chem.* **1992**, *26*, 879.
(49) Helgaker, T.; Jensen, H. J. A.; Jørgensen, P.; Olsen, J.; Ruud, K.; Ågren, H.; Andersen, T.; Bak, K. L.; Bakken, V.; Christiansen, O.; Dahle, P.; Dalskov, E. K.; Enevoldsen, T.; Heiberg, H.; Hettema, H.; Jonsson, D.; Kirpekar, S.; Kobayashi, R.; Koch, H.; Mikkelsen, K. V.; Norman, P.; Packer, M. J.; Saue, T.; Taylor, P. R.; Vahtras, O. *DALTON, an ab initio electronic structure program*, release 1.0; 1997.
(50) Ahlrichs, R.; Bär, M.; Häser, M.; Horn, H.; Kölmel, C. *Chem. Phys. Lett.* **1989**, *162*, 165.
(51) Dunning, T. H. *J. Chem. Phys.* **1989**, *90*, 1007.
(52) Karlström, G.; Lindh, R.; Malmqvist, P. A.; Roos, B. O.; Ryde, U.; Veryazov, V.; Widmark, P. O.; Cossi, M.; Schimmelpfennig, B.; Neogrady, P.; Seijo, L. *Comput. Mater. Sci.* **2003**, *28*, 222.
(53) Spek, A. L. *J. Appl. Crystallogr.* **2003**, *36*, 7.
(54) Abouaf, R.; Pommier, J.; Dunet, H. *Chem. Phys. Lett.* **2003**, *381*, 486.
(55) Bomble, Y. J.; Sattelmeyer, K. W.; Stanton, J. F.; Gauss, J. *J. Chem. Phys.* **2004**, *121*, 5236.
(56) Müller, T.; Dallos, M.; Lischka, H. *J. Chem. Phys.* **1999**, *110*, 7176.
(57) Barbatti, M.; Lischka, H. *J. Phys. Chem. A* **2007**, *111*, 2852.
(58) Barbatti, M.; Sellner, B.; Aquino, A. J. A.; Lischka, H. Nonadiabatic excited-state dynamics of aromatic heterocycles: toward the time-resolved simulation of nucleobases. In *Radiation Induced Molecular Phenomena in Nucleic Acid*; Shukla, M. K., Leszczynski, J., Eds.; Springer: Netherlands, 2008.
(59) Zechmann, G.; Barbatti, M. *Int. J. Quantum Chem.* **2008**, *108*, 1266.
(60) Barbatti, M.; Vazdar, M.; Aquino, A. J. A.; Eckert-Maksic, M.; Lischka, H. *J. Chem. Phys.* **2006**, *125*, 164323.
(61) Perun, S.; Sobolewski, A. L.; Domcke, W. *Chem. Phys.* **2005**, *313*, 107.
(62) Barbatti, M.; Aquino, A. J. A.; Lischka, H. *Chem. Phys.* **2008**, *349*, 278.
(63) Antol, I.; Eckert-Maksic, M.; Barbatti, M.; Lischka, H. *J. Chem. Phys.* **2007**, *127*, 234303.
(64) Sobolewski, A. L.; Domcke, W. *Chem. Phys.* **2000**, *259*, 181.
(65) Perun, S.; Sobolewski, A. L.; Domcke, W. *J. Am. Chem. Soc.* **2005**, *127*, 6257.
(66) Ashfold, M. N. R.; Cronin, B.; Devine, A. L.; Dixon, R. N.; Nix, M. G. D. *Science* **2006**, *312*, 1637.
(67) Barbatti, M.; Ruckenbauer, M.; Szymczak, J. J.; Aquino, A. J. A.; Lischka, H. *PhysChemChemPhys* **2008**, *10*, 482.
(68) Barbatti, M.; Aquino, A. J. A.; Lischka, H. *Mol. Phys.* **2006**, *104*, 1053.
(69) Zechmann, G.; Barbatti, M.; Lischka, H.; Pittner, J.; Bonačić-Koutecký, V *Chem. Phys. Lett.* **2006**, *418*, 377.

JP804309X